

KEK-TH-1022  
PITHA-05-09  
OU-HET 532  
hep-ph/0506249

## Enhancement of $W^\pm H^\mp$ Production at Hadron Colliders in the Two Higgs Doublet Model

Eri Asakawa<sup>a 1</sup>, Oliver Brein<sup>b 2</sup> and Shinya Kanemura<sup>c 3</sup>

<sup>a</sup> *Theory Group KEK, Tsukuba, Ibaraki, 305-0801, Japan*

<sup>b</sup> *Institut für Theoretische Physik E, RWTH Aachen D-52056 Aachen, Germany*

<sup>c</sup> *Department of Physics, Osaka University, Toyonaka, Osaka 560-0043, Japan*

### Abstract

We discuss the associated  $W^\pm H^\mp$  production at the CERN Large Hadron Collider. The dependence of the hadronic cross section on the Higgs sector parameters is investigated in detail in the framework of the general Two Higgs Doublet Model (THDM). We study the possible enhancement of the THDM prediction for the cross section compared to the prediction of the Minimal Supersymmetric Standard Model (MSSM). We find regions in the THDM parameter space where the THDM prediction can exceed the one of the MSSM by two orders of magnitude. These regions of large cross section are in agreement with theoretical bounds on the model, derived from the requirement of vacuum stability and perturbative unitarity, and are not excluded by experimental constraints.

---

<sup>1</sup>E-mail: eri@yukawa.kyoto-u.ac.jp; Address after April 2005: YITP, Kyoto University.

<sup>2</sup>E-mail: brein@physik.rwth-aachen.de

<sup>3</sup>E-mail: kanemu@het.phys.sci.osaka-u.ac.jp

# 1 Introduction

Spontaneous symmetry breakdown is a necessity in theoretical descriptions of electroweak phenomena. We know of no other way to unite the principle of gauge symmetry with the description of massive vector bosons. While gauge symmetry is required in the theoretical description of electroweak physics in order to get meaningful predictions at the quantum level, the existence of the massive vector bosons  $W^\pm$  and  $Z$  is an experimental fact since their discovery at LEP. Although the Standard Model (SM) of particle physics is well tested even at the quantum level in several cases, there is no sign of the Higgs boson so far. Up to now only bounds on the Higgs boson mass(es) could be extracted from high energy collision experiments. These bounds are always obtained under the hypothesis that a certain model of the Higgs sector describes the data. However, as there is no Higgs signal yet, the choice of model for the Higgs sector is rather unconstrained. Therefore, extensions of the SM Higgs sector have to be considered seriously in phenomenology.

Such extended Higgs sectors would also be considered as low energy effective theories of new physics models beyond the SM, which are proposed to describe physics at higher energies than the electroweak scale. Supersymmetry is one of the examples for such new physics scenarios, which requires at least two scalar doublet fields in the Higgs sector. Apart from supersymmetry, there are varieties of new physics models most of which have been proposed during the last decade, such as extra dimension models [1], the little Higgs models [2] and others. The low energy effective theories for some of these models predict extended Higgs sectors. Non-minimal Higgs sectors are also considered in models with strongly interacting dynamics for the symmetry breaking such as top-color models [3]. Furthermore, some models designed to explain tiny neutrino masses [5], CP-violation [4], and electroweak baryogenesis [6] also require an extension of the minimal Higgs sector of the SM.

From the phenomenological point of view, such extensions of the Higgs sector have to meet two major restrictions from experiments: a) the electroweak rho-parameter has to be one up to a few per mille and b) large flavor changing neutral currents (FCNC) have to be absent. By discarding models which do not meet these criteria or meet them only by fine-tuned choices of model parameters, one ends up with models which have  $\rho = 1$  and no FCNC at tree-level. In particular, it is well known that all models with an arbitrary number of isospin  $SU(2)$ -doublets and -singlets can be of that type [8] by imposing discrete symmetries to avoid FCNC.

The Two Higgs Doublet Model (THDM) is the model with the minimal extension of the SM Higgs sector, which leads to new phenomena in the matter and gauge field sector<sup>4</sup>. In the THDM, tree level FCNC can be eliminated by imposing a discrete symmetry, under which there are two possibilities depending on its charge assignment [7, 8]; i.e., (Type I) only one of the Higgs doublets gives mass to the fermions, and (Type II) one gives mass to the up-type quarks and the other to the down-type quarks and charged leptons. The Higgs sector of the minimal supersymmetric extension of the SM (MSSM) is a special case of

---

<sup>4</sup>A mere addition of scalar isospin-singlets would only modify the Higgs boson self-interactions.

the type II THDM. As the general THDM may be considered as a low energy description of other new physics models, it is an interesting question whether one can distinguish experimentally between the MSSM and such a model.

The question about the new physics model underlying the Higgs sector can be addressed only after the existence of Higgs particles has been established experimentally. The Higgs search program at high energy colliders divides basically into three steps: a) discovery of the Higgs boson(s), b) measurement of fundamental properties like its mass, width, spin, parity etc., and c) determination of the underlying model of the Higgs sector; i.e., the measurement of the Higgs bosons' couplings to other particles and to themselves and the measurement of quantum effects. The current paper deals with an example which might contribute to last step. As is well known, the discovery of a charged Higgs boson would be an unambiguous sign of an extended Higgs sector. At hadron colliders, the main production mechanisms are top-quark decay in top-quark pair production if  $m_{H^\pm} < m_t + m_b$  [9] and single  $H^-$  ( $H^+$ ) production by bottom-gluon scattering and gluon fusion ( $gb \rightarrow tH^-$ ,  $gg \rightarrow H^-t\bar{b}/H^- \bar{\tau}\nu_\tau$  and charge conjugated) if  $m_{H^\pm} > m_t + m_b$  [10].

In this paper, we study  $H^\pm W^\mp$  production at hadron colliders. This process is not a main production process for the charged Higgs boson, but it turns out to be strongly model dependent in contrast to the main production mechanisms. After the discovery of a charged Higgs boson, the observation of this process could potentially help to unravel the underlying model of the Higgs sector. The main purpose of this paper is to demonstrate this possibility by studying the predictions of the MSSM and THDM in comparison. The MSSM prediction for  $H^\pm W^\mp$  production at hadron colliders has been studied by several authors [11, 12, 13, 14, 15, 16, 17]. Especially, the detectability of  $H^\pm W^\mp$  production at the CERN Large Hadron Collider (LHC) in the framework of the MSSM has been studied in Ref. [17] which concludes with rather poor prospects. We reconsider this process in the THDM, and study discriminative features with respect to the MSSM. The cross section is evaluated in the THDM in a wide parameter range. We exclude areas of parameter space by the requirement of vacuum stability [18, 19] and perturbative unitarity [20, 21, 22].<sup>5</sup> Experimental results, such as on the rho-parameter [27], the muon anomalous magnetic moment [29] and  $b \rightarrow s\gamma$  [24] are also taken into account. We find that in the regions of parameter space which are not excluded by the theoretical requirements and the experimental constraints, a large enhancement of the hadronic cross section can be obtained as compared to the MSSM prediction. Therefore, in certain cases, the signal can be detectable at the LHC.

The rest of the paper is organized as follows. In section 2, we briefly review the THDM and present the restrictions for the THDM parameters, derived from theoretical constraints and present experimental data. Section 3 deals with the essentials of the  $W^\pm H^\mp$  production process at hadron colliders. In Section 4, we discuss the THDM prediction for the production cross section in comparison with the MSSM prediction, having regard to all the parameter restrictions discussed in section 2. Our conclusions and the appendix follow.

---

<sup>5</sup>Similar approaches are seen in Refs.[23]

## 2 THDM parameters

The THDM contains two scalar weak isospin doublets  $\Phi_1, \Phi_2$  with hypercharge  $Y(\Phi_i) = +1$ . Conventionally, there are two types of THDMs which are characterized by the way the scalar doublets are coupled to fermions. In type I all fermions couple to one doublet, while in type II up- and down-type fermions couple to different doublets [8]. In either type FCNC are automatically absent at tree level [7]. Here, we consider a THDM of type II. The Higgs sector of the CP-conserving THDM can be described by the following potential [8]:

$$V(\Phi_1, \Phi_2) = \lambda_1(\Phi_1^\dagger\Phi_1 - v_1^2)^2 + \lambda_2(\Phi_2^\dagger\Phi_2 - v_2^2)^2 + \lambda_3[(\Phi_1^\dagger\Phi_1 - v_1^2) + (\Phi_2^\dagger\Phi_2 - v_2^2)]^2 \\ + \lambda_4[(\Phi_1^\dagger\Phi_1)(\Phi_2^\dagger\Phi_2) - (\Phi_1^\dagger\Phi_2)(\Phi_2^\dagger\Phi_1)] + \lambda_5[\text{Re}(\Phi_1^\dagger\Phi_2) - v_1v_2]^2 + \lambda_6[\text{Im}(\Phi_1^\dagger\Phi_2)]^2, \quad (1)$$

with two real parameters with mass dimension one ( $v_1, v_2$ ) and 6 dimensionless real parameters ( $\lambda_1, \dots, \lambda_6$ ). This potential has its minimum at  $\Phi_i = (0, v_i)^T$  ( $i = 1, 2$ ). Re-expressing the fields such that the new degrees of freedom vanish at the minimum and diagonalizing the resulting bilinear scalar interaction terms one obtains a separation of the physical and unphysical spectrum of the model. The physical spectrum of the Higgs sector of the CP-conserving THDM consists of 3 neutral Higgs bosons, 2 CP-even ( $h^0, H^0$ ) and one CP-odd ( $A^0$ ), and two charged ones ( $H^+, H^-$ ). The 8 free parameters of the Higgs sector can also be chosen to be the modulus of the vacuum expectation value  $v = \sqrt{v_1^2 + v_2^2} = \sqrt{2^{-3/2}G_F^{-1}}$ , the masses of the Higgs bosons,  $m_{h^0}, m_{H^0}, m_{A^0}$  and  $m_{H^\pm}$ , the mixing angles  $\alpha$  and  $\beta$  used in the diagonalization of the Higgs boson propagator matrices, and  $\lambda_5$ . The discrete symmetry of the Higgs potential (e.g.  $\Phi_1 \rightarrow \Phi_1, \Phi_2 \rightarrow -\Phi_2$ ) is broken by a mass-dimension two term proportional to  $M^2 = v^2\lambda_5$ . The physical meaning of  $M$  is the cut-off scale of the effective SM when  $M \gg v$ . In the following, we review the constraints which we take into account in our numerical study.

### 1. theoretical constraints

The coupling constants in Eq. (1) can be restricted by imposing theoretical requirements for the consistency of the model. Here, we use the conditions derived from the requirement of vacuum stability [18, 19] and perturbative unitarity [20, 21, 22] for the tree-level coupling constants. The condition of vacuum stability is given by

$$\lambda_1 + \lambda_3 > 0, \quad \lambda_2 + \lambda_3 > 0, \\ 2\sqrt{(\lambda_1 + \lambda_3)(\lambda_2 + \lambda_3)} + 2\lambda_3 + \lambda_4 + \min[0, \lambda_5 - \lambda_4, \lambda_6 - \lambda_4] > 0. \quad (2)$$

The requirement of perturbative unitarity demands that the magnitudes of all tree-level S-wave amplitudes for the elastic scattering of longitudinally polarized gauge and Higgs bosons stay within the limit set by unitarity. In our analysis, we consider the 14 neutral channels [21]. The expressions for the eigenvalues of the scattering matrix,  $a_i$  ( $i = 1, \dots, 14$ ), are summarized in Appendix B.

### 2. rho-parameter constraint

The electroweak rho-parameter, which is one at tree-level in the SM, is a scheme-dependent

quantity beyond the leading order in perturbation theory. For models beyond the SM the definition  $\rho = \rho_0 \rho_{\text{SM}} = m_W^2 / (m_Z^2 c_w^2)$  is used in Ref. [27] in the  $\overline{MS}$  scheme, where  $\rho_{\text{SM}}$  absorbs all SM radiative corrections and  $\rho_0$  parameterizes the extra new physics contributions, i.e.  $\rho_0 = 1$  if the new physics contributions vanish. A value for  $\rho_0$  has been obtained from a global fit to electroweak precision observables [27],

$$\rho_0 = 0.9998_{-0.0010}^{+0.0025}, \quad (3)$$

where the error bar given above is at the  $2\sigma$  level. The only difference between the SM and the THDM is the Higgs sector. Thus, we can decompose the contributions to  $\rho$  ( $\equiv \rho_{\text{THDM}}$ ) into all contributions containing at least one virtual Higgs boson,  $\rho_{\text{THDM,Higgs}}$ , and all others, which coincide with the SM contributions:  $\rho_{\text{THDM}} = \rho_{\text{SM,no Higgs}} + \rho_{\text{THDM,Higgs}}$ . Likewise, the SM rho-parameter decomposes into  $\rho_{\text{SM}} = \rho_{\text{SM,no Higgs}} + \rho_{\text{SM,Higgs}}$ . Hence, the deviation  $\delta\rho_0 = \rho_0 - 1$  at the one-loop level is just the difference  $\delta\rho_0 = \rho_{\text{THDM,Higgs}} - \rho_{\text{SM,Higgs}}$ . In our study, we constrain the THDM parameters such that the one-loop prediction for  $\delta\rho_0$  stays within the range indicated by Eq. (3); i.e.,  $-0.0012 \leq \delta\rho_0 \leq 0.0023$ . The specific formulas for this difference can be found in Refs. [8, 30].

### 3. constraint from $a_\mu$

The latest results on the measurement of the anomalous magnetic moment of the muon [29],  $a_\mu$ , suggest that the difference between measurement and SM prediction is [27]:

$$\Delta a_\mu := a_\mu^{\text{exp.}} - a_\mu^{\text{SM}} = (25.7 \pm 8.54 \pm 4.90) \cdot 10^{-10}, \quad (4)$$

where the first error is the total experimental error and the second is the theoretical uncertainty of the SM prediction. In the THDM, radiative corrections to processes without any external Higgs bosons always split into contributions without any virtual Higgs boson and others which involve at least one virtual Higgs boson. Thus, the difference between the THDM and the SM prediction for  $a_\mu$  is given by the difference in the Higgs sector contribution,  $\delta a_\mu = a_\mu^{\text{THDM,Higgs}} - a_\mu^{\text{SM,Higgs}}$ . As is well known, the leading order virtual Higgs contributions are suppressed by two Higgs-muon Yukawa couplings [34]. At the two-loop level, a virtual Higgs boson can couple to the muon and one internal loop of heavy particles, e.g. Fermions with a much larger Yukawa coupling. This is the class of so-called ‘‘Barr-Zee’’ type Feynman graphs [35]. Their contributions to  $a_\mu$  exceed the leading order virtual Higgs contributions by several orders of magnitude. In our calculation of  $\delta a_\mu$ , we include all relevant one-loop contributions [34] and all Barr-Zee type two-loop contributions with a closed fermion or charged Higgs boson loop [36]. Assuming the validity of the THDM, we constrain its parameter space such that the value of  $\delta a_\mu$  stays close to  $\Delta a_\mu$  within the  $2\sigma$  error bars; i.e.,  $-1.2 \cdot 10^{-10} \leq \delta a_\mu \leq 52.6 \cdot 10^{-10}$ .

### 4. constraint from $b \rightarrow s\gamma$

In our discussion, we take a charged Higgs boson with  $m_{H^\pm} = 400 \text{ GeV}$ . Therefore, the limits for new physics contributions to the decay  $b \rightarrow s\gamma$  are respected [24, 25] for all values of  $\tan\beta$  which we discuss.

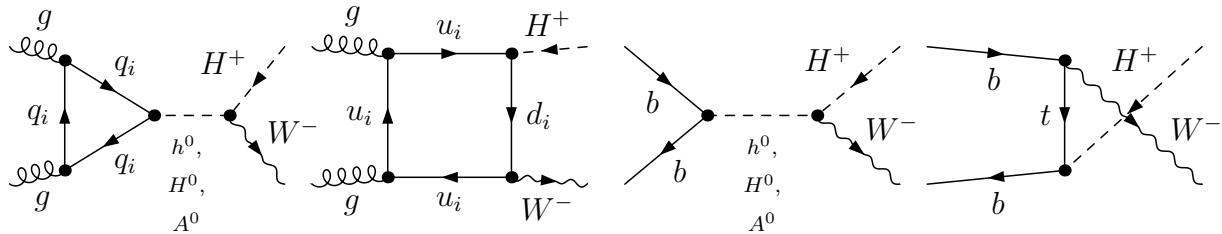


Figure 1: Typical Feynman graphs for the partonic processes gluon fusion and  $b\bar{b}$  annihilation contributing to  $W^\pm H^\mp$  production at a hadron collider. For gluon fusion there are in total two triangle-type topologies for each quark flavor and six box-type topologies for each quark generation.

### 3 $W^\pm H^\mp$ production at hadron colliders

#### Partonic processes

In the framework of the parton model, there are two distinct subprocesses which contribute to the production of a charged Higgs boson,  $H^\pm$ , and a electroweak gauge boson,  $W^\mp$ :  $b\bar{b}$ -annihilation,

$$b(k, \alpha, \sigma) + \bar{b}(\bar{k}, \beta, \bar{\sigma}) \rightarrow W^-(p, \lambda) + H^+(\bar{p}) , \quad (5)$$

and gluon fusion,

$$g(k, a, \sigma) + g(\bar{k}, b, \bar{\sigma}) \rightarrow W^-(p, \lambda) + H^+(\bar{p}) . \quad (6)$$

In- and outgoing momenta of the initial and final state particles are denoted by  $k, \bar{k}$  and  $p, \bar{p}$  respectively, the helicities of the initial state gluons or quarks by  $\sigma, \bar{\sigma}$  and of the final state  $W$  by  $\lambda$ .  $a, b$  denote the gluon SU(3)-color indices and  $\alpha, \beta$  the quark color indices. The square of the center of mass energy of the parton system is then given by  $\hat{s} = (k + \bar{k})^2 = (p + \bar{p})^2$ .

The leading order  $b\bar{b}$ -annihilation amplitude (5) consists of two types of tree-level Feynman graphs: (i) graphs with s-channel exchange of a neutral Higgs boson and (ii) graphs with a t-channel virtual top quark (see Fig. 1). The amplitude for the gluon-fusion process (6) is given in leading order in perturbation theory by a set of one-loop Feynman graphs (see Fig.1). Gluon fusion, though loop-induced, may contribute significantly to the cross section, because of the large number of gluon-gluon collisions with sufficient center-of-mass energy to exceed the production threshold at high energy hadron colliders.

Associated  $W^\pm H^\mp$  production via  $b\bar{b}$  annihilation and the gluon fusion have been discussed at first for a THDM with MSSM parameter values including the loop contributions from top and bottom quarks in the approximation  $m_b = 0$  [11]. Therefore, this study only covered MSSM scenarios with small  $\tan\beta$  and scalar quark masses which are sufficiently heavy to decouple from the loop contributions. This work has been extended by including

squark-loop contributions and a non-zero  $b$ -quark mass [12, 13], thus allowing the investigation of the process for arbitrary scalar quark masses and values of  $\tan\beta$ . The gluon-fusion channel in the MSSM has also been studied in Ref. [14] and for the  $b\bar{b}$ -annihilation channel the supersymmetric electroweak corrections [15] and the QCD corrections [16] at one-loop order are known. A phenomenological study of the signal-to-background ratio for the semi-leptonic signature  $W^\pm H^\mp \rightarrow W^\pm tb \rightarrow b\bar{b}W^+W^- \rightarrow b\bar{b}jjl + \text{missing energy/momentum}$  for a MSSM-like THDM (neglecting the box-loop contributions) has been performed in Ref. [17]. The authors of Ref. [17] showed that the background rate, which mainly comes from  $t\bar{t}$  production, overwhelms the signal rate by two to three orders of magnitude. A generic feature of the MSSM gluon-fusion amplitude is a strong negative interference between triangle- and box-type quark-loop Feynman graphs. This behavior, already noted in Ref. [11], is due to the relations between Higgs masses in the MSSM, and leads to a much smaller cross section than one would obtain by squaring triangle- or box-type quark-loops alone.

The  $W^\pm H^\mp$  production cross section at hadron colliders in the framework of the general THDM has not been studied in the literature<sup>6</sup>. We discuss this cross section in the framework of a general CP-conserving type II THDM, which contains the MSSM Higgs sector as a special case and therefore allows for straightforward comparisons between the models. Dropping the superpartner contributions and allowing the Higgs boson masses ( $m_{h^0}, m_{H^0}, m_{A^0}, m_{H^\pm}$ ) and the mixing angle in the Higgs sector ( $\alpha$ ) to be free parameters, one obtains the expression for the partonic cross section  $\hat{\sigma}_{gg \rightarrow W-H^\pm}$  in the THDM from the results of Ref. [13]. The formulas for  $\hat{\sigma}_{b\bar{b} \rightarrow W-H^\pm}$  in the THDM can be taken over e.g. from the MSSM calculation in Ref. [12]. As all Higgs boson masses in the THDM are free parameters, it may occur that their values lie above the threshold  $m_W + m_{H^\pm}$ . This gives rise to resonant s-channel contributions. Therefore, we calculate the widths  $\Gamma_\Phi$  ( $\Phi = h^0, H^0, A^0$ ) of the neutral Higgs bosons in leading order approximation and introduce them in the s-channel propagators of the Feynman graphs of the  $b\bar{b}$ -annihilation and gluon-fusion process. Specifically, we make the following replacements for the propagator terms of neutral Higgs bosons in the formulas of Refs. [12, 13]:

$$\frac{1}{\hat{s} - m_\Phi^2} \rightarrow \frac{1}{\hat{s} - m_\Phi^2 + im_\Phi\Gamma_\Phi}.$$

In the THDM, there are parameter combinations in which one Higgs boson can decay into two others which gives a large contribution to its width. We take this into account by including all self-interaction contributions to the total width of the neutral Higgs bosons. The partial widths of neutral Higgs bosons associated with decays into SM particles are well known and have been taken over from Ref. [8] and the ones associated with decays into Higgs particles are given by

$$\Gamma(\Phi_1 \rightarrow \Phi_i\Phi_j) = \frac{\sqrt{m_1^4 + m_i^4 + m_j^4 - 2m_1^2m_i^2 - 2m_1^2m_j^2 - 2m_i^2m_j^2}}{16\pi m_1^3(1 + \delta_{ij})} |g_{\Phi_1\Phi_i\Phi_j}|^2,$$

---

<sup>6</sup>A preliminary study of the THDM gluon-fusion process has been presented in Ref. [26].

with the Higgs self-couplings  $g_{\Phi_1\Phi_i\Phi_j}$  listed in appendix A.

We describe above how to obtain the expressions for the partonic cross sections from the formulas of Refs. [12, 13]. However, our calculation of the partonic cross sections has been performed independently with the help of the computer programs FeynArts and FormCalc [31].

### Hadronic cross section

The hadronic inclusive cross section for  $W^-H^+$  production in proton-proton collisions at a total hadronic center of mass energy  $\sqrt{S}$  can be written as a convolution [32],

$$\sigma_{pp \rightarrow W^-H^+X} = \sum_{\{n,m\}} \int_{\tau_0}^1 d\tau \frac{d\mathcal{L}_{nm}^{pp}}{d\tau} \hat{\sigma}_{nm \rightarrow W^-H^+}(\tau S, \alpha_S(\mu_R)) = \sum_{\{n,m\}} \int_{\sqrt{\hat{s}_0}}^{\sqrt{S}} d\sqrt{\hat{s}} \frac{d\sigma_{nm}}{d\sqrt{\hat{s}}}, \quad (7)$$

with the parton luminosity

$$\frac{d\mathcal{L}_{nm}^{pp}}{d\tau} = \int_{\tau}^1 \frac{dx}{x} \frac{1}{1 + \delta_{nm}} \left[ f_{n/p}(x, \mu_F) f_{m/p}\left(\frac{\tau}{x}, \mu_F\right) + f_{m/p}(x, \mu_F) f_{n/p}\left(\frac{\tau}{x}, \mu_F\right) \right], \quad (8)$$

where  $f_{n/p}(x, \mu_F)$  denotes the density of partons of type  $n$  in the proton carrying a fraction  $x$  of the proton momentum at the scale  $\mu_F$ . In our case, there are two parton subprocesses contributing to inclusive  $W^-H^+$  hadroproduction; gluon fusion and  $b\bar{b}$ -annihilation. The numerical evaluation has been carried out with the leading order MRST parton distribution functions [33] and with the renormalization and factorization scale  $\mu_R$  and  $\mu_F$  chosen equal to the threshold,  $m_W + m_{H^\pm}$ .

## 4 Numerical Results

We take  $m_Z$ ,  $m_W$  and  $G_F$  as the input electroweak parameters, and use values  $m_Z = 91.1876$  GeV,  $m_W = 80.424$  GeV and  $G_F = 1.16637 \times 10^{-5}$  GeV<sup>-2</sup> [27]. For the strong coupling constant  $\alpha_S(\mu_R)$ , we use the formula including the two-loop QCD corrections for  $n_f = 5$  with  $\Lambda_{QCD}^5 = 174$  MeV which can be found in [27]. The mass of the top and bottom quarks are fixed here as  $m_t = 174.3$  GeV and  $m_b = 4.7$  GeV.

In our exemplary discussion we take one MSSM scenario as a reference, characterized by the following settings of MSSM parameters:

$$\begin{aligned} M_{\text{SUSY}} &= M_{\tilde{Q}} = M_{\tilde{U}} = M_{\tilde{D}} = M_{\tilde{L}} = M_{\tilde{E}} = 1000 \text{ GeV}, \\ \mu &= 300 \text{ GeV}, \\ X_t &= A_t - \mu \cot \beta = -1000 \text{ GeV}, \\ A_u &= A_d = A_c = A_s = A_b = 0, \end{aligned} \quad (9)$$

where  $M_{\text{SUSY}}$  is a common squark mass scale,  $\mu$  is the Higgs-superfield mass parameter in the superpotential,  $X_t$  the mixing parameter in the stop sector, and the  $A_q$  are trilinear Higgs couplings to squarks<sup>7</sup>. We set  $m_{H^\pm} = 400$  GeV throughout the paper and calculate

<sup>7</sup>For more details on these parameters in our convention see Ref. [13].

	$\tan\beta$			
	1.5	3	6	10
$m_{h^0}$ [GeV]	85.6	105.5	115.2	117.6
$m_{H^0}$ [GeV]	404.7	396.8	393.3	392.4
$m_{A^0}$ [GeV]	391.8	391.8	391.8	391.8
$m_{H^\pm}$ [GeV]	400.0	400.0	400.0	400.0
$\alpha$ [rad]	-0.63465	-0.36335	-0.19050	-0.11558
$\sigma_{pp \rightarrow W^\pm H^\mp}^{\text{MSSM}}$ [fb]	37.78	9.48	3.08	2.96

Table 1: MSSM values for the Higgs masses and the mixing angle  $\alpha$ . The prediction for the hadronic cross section in our MSSM reference scenario (see Eq. (9)) are also shown.

the mass of the MSSM CP-odd Higgs boson using the tree-level relation  $m_{A^0}^2 = m_{H^\pm}^2 - m_W^2$ . A THDM with all parameters set to the MSSM values, especially  $M = m_{A^0}$ , is called MSSM-like. In Table 1, we list the MSSM values for the Higgs masses and the mixing angle  $\alpha$ . Note that the case  $\tan\beta = 1.5$  in the MSSM is actually ruled out by the latest LEP direct search results [28].

Fig. 2 shows a comparison between the THDM and MSSM predictions for the differential hadronic cross section

$$\frac{d\sigma_{nm}}{d\sqrt{\hat{s}}} = \frac{2\sqrt{\hat{s}}}{S} \frac{d\mathcal{L}_{nm}^{pp}}{d\tau} \Big|_{\tau=\frac{\sqrt{\hat{s}}}{S}} \hat{\sigma}_{nm \rightarrow W^- H^+}(\sqrt{\hat{s}}, \alpha_S(\mu_R)), \quad (10)$$

as a function of  $\sqrt{\hat{s}}$ . In the linear plot on the right hand side, one can see that the  $gg$ - and  $b\bar{b}$ -channel contribution to the hadronic cross section is of comparable size, whereas the partonic cross section  $\hat{\sigma}_{gg \rightarrow W^- H^+}$  is orders of magnitude lower than  $\hat{\sigma}_{b\bar{b} \rightarrow W^- H^+}$ . This is caused by the enhancement factor due to the large number of gluon-gluon collisions at high energy hadron colliders. In Fig. 2, two THDM scenarios are displayed: one (scenario A) is completely MSSM-like, with the settings  $m_{H^\pm} = 400$  GeV and  $\tan\beta = 6$ , and the other (scenario B) coincides with the first one except for the choice  $m_{A^0} = 4m_{A^0}^{\text{MSSM}}$ , which leads to the peak at  $\sqrt{\hat{s}} = m_{A^0} \approx 1600$  GeV. We also show in Fig. 2 the MSSM prediction by thin solid and dashed lines further marked by circles and boxes respectively. Clearly, there is almost no deviation from the MSSM-like THDM except for squark threshold effects around  $\sqrt{\hat{s}} \approx 2000$  GeV which can be seen in the left plot.

In order to demonstrate the strong negative interference in the MSSM gluon-fusion process, we display artificial MSSM predictions for this process using only Feynman graphs either of box-type (thin dotted lines) or of triangle-type (thin dot-dashed lines) in the calculation. Those are more than one order of magnitude larger than the full result over a wide range of  $\sqrt{\hat{s}}$  (see Fig. 2, left plot). From Fig. 2, we learn that we can get a much larger cross section near to the production-threshold region by near-decoupling of the triangle-type graphs. In this region the cross section in the THDM scenario B is close to the “only box graphs” MSSM result. However, the resonant peak far off the production

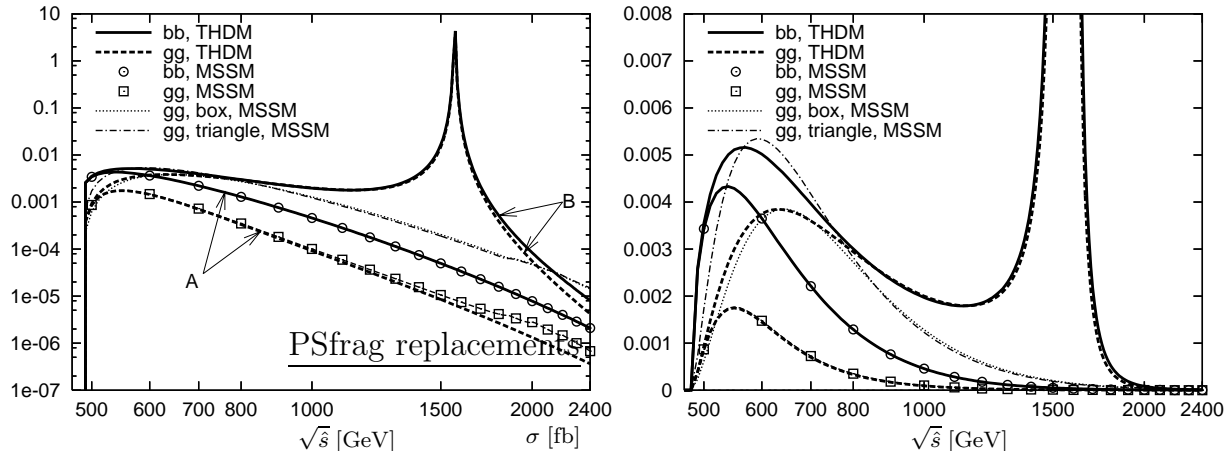


Figure 2: The differential hadronic cross section  $d\sigma_{nm}/d\sqrt{\hat{s}}$  in fb/GeV for  $W^-H^+$  production is plotted versus  $\sqrt{\hat{s}}$ . Thick and thin lines show THDM and MSSM results respectively. Dashed and solid lines show the  $gg$  and  $b\bar{b}$  contribution respectively. Two THDM scenarios are displayed: one with all parameters MSSM-like (A) and one with  $m_A = 4m_A^{\text{MSSM}}$  (B). The MSSM prediction is highlighted by circles ( $b\bar{b}$ ) and squares ( $gg$ ). Also shown is the MSSM “prediction” for the  $gg$  cross section only using box- (dotted lines) or triangle-type (dot-dashed) Feynman graphs in the calculation.

threshold also contributes significantly to the total hadronic cross section. Naively, one could have thought the peak far off would not contribute significantly because of the much lower parton luminosity.

The hadronic cross section  $\sigma_{pp \rightarrow W^\pm H^\mp}$  as a function of  $m_{A^0}$  and  $m_{H^0}$ , for  $\tan\beta = 1.5, 3, 6, 10$  is displayed for  $M^2 = m_{A^0}^2$  in Fig. 3,  $M^2 = m_{A^0}^2/2$  in Fig. 4, and  $M^2 = 0$  in Fig. 5. In all Figures the exclusion limits (thick lines) are superimposed on the cross section contours (thin lines). As a generic feature, the cross section rises strongly, if  $m_{A^0}$  or  $m_{H^0}$  becomes larger than  $m_W + m_{H^\pm} \approx 480$  GeV, with a maximum well above the contour where resonant  $A^0$ - and  $H^0$ -exchange contributions are possible. This behavior is due to two enhancement effects: a) resonant propagator contributions for  $m_{A^0}, m_{H^0} > 480$  GeV and b) a reduction of the strong negative interference if one propagator starts to decouple from the production threshold. The variation of the cross section with  $M$  is due to the  $M$ -dependence of the Higgs self-coupling constants (see Appendix A), which enter the widths of  $A^0$  and  $H^0$ .

Imposing the constraints described in the previous chapter, we focus on the remaining areas in Figs. 3 to 5 which are allowed by all constraints. Remarkably, there remains an allowed region in all cases. For  $M^2 = m_{A^0}^2$  (see Fig. 3) the cross section in the allowed region varies roughly in the range 20 to 1200 fb for  $\tan\beta = 1.5, 10$  to 50 fb for  $\tan\beta = 3$  and around the MSSM value for  $\tan\beta = 6$  and 10. For  $M^2 = m_{A^0}^2/2$  (see Fig. 4) the lower bound of the cross section is similar to the previous case, while 1000 fb are possible for  $\tan\beta = 1.5, 3$  and 6, and 20 fb for  $\tan\beta = 10$ , which is still about 60 times the MSSM cross section. Depending on  $\tan\beta$ , the case  $M^2 = 0$  is strongly constrained to rather low

values of  $m_{H^0}$ . Because of the rho-parameter constraint, the allowed areas for  $\tan\beta = 3, 6$  and 10 have a cross section below the corresponding MSSM scenario but of the same order. For  $\tan\beta = 1.5$  again large variations of the cross section are possible, roughly between 40 and 1500 fb.

## 5 Conclusions

We have discussed the  $H^\pm W^\mp$  production at hadron colliders in the framework of a general type II THDM and compared the predictions with the MSSM. We find that the THDM prediction for the hadronic cross section can be completely different from the MSSM prediction. Specifically, we find regions in parameter space where the cross section exceeds 1000 fb. These regions of large cross section are in agreement with theoretical constraints, vacuum stability and perturbative unitarity, and are not excluded by experimental constraints from measurements of the rho-parameter and the muon magnetic moment. In Ref. [17], it is discussed that the size of the MSSM cross section would not be sufficient to detect this process at the LHC. An enhanced cross section in a general THDM scenario, examples of which are shown in this paper, would give a nice possibility to see the  $H^\pm W^\mp$  signal at the LHC. Certainly, the  $H^\pm W^\mp$  cross section is not a discovery channel for the charged Higgs at hadron colliders. However, once a charged Higgs boson has been discovered, its observation will help to gain information on the underlying model of the Higgs sector. One should keep in mind that there are many other new physics models, apart from supersymmetry, which can be described by a THDM as a low energy effective theory. It would be valuable to study the detectability of  $H^\pm W^\mp$  production in the framework of the general THDM by realistic simulation. We provide a FORTRAN code for general use.

*Acknowledgments.* S. K. would like to thank for the hospitality and support during his stay in Aachen, where this paper was completed. E. A. was supported by the Japan Society for the Promotion of Science. S. K. was also supported in part by Grant-in-Aid of the Ministry of Education, Culture, Sports, Science and Technology, Government of Japan, grant No. 17043008. This work is supported in part by the Deutsche Forschungsgemeinschaft Sonderforschungsbereich/Transregio 9, Computergestützte Theoretische Teilchenphysik.

# Appendix

## A Higgs self-couplings

We display here only those triple-Higgs couplings which are needed in the evaluation of the corresponding partial decay widths of the neutral Higgs bosons. The case of a MSSM-like Higgs sector is recovered if the MSSM values are chosen for  $m_{h^0}, m_{H^0}, \alpha$  and  $M$  is set to  $m_{A^0}$ . The shorthands  $s_\psi := \sin \psi, c_\psi := \cos \psi$  are used.

$$\begin{aligned}
g_{h^0 H^0 H^0} &= \sqrt{G_F} \left\{ \frac{M^2}{\sqrt{2}} \left( s_{\alpha-\beta} - 3 \frac{s_\alpha}{c_\beta} + 3 s_\alpha^2 \frac{c_{\alpha-\beta}}{c_\beta s_\beta} \right) + (4m_{H^0}^2 + 2m_{h^0}^2) \left( \frac{s_\alpha}{c_\beta} - s_\alpha^2 \frac{c_{\alpha-\beta}}{c_\beta s_\beta} \right) \right\}, \\
g_{h^0 A^0 A^0} &= \sqrt{G_F} \left\{ \frac{M^2}{\sqrt{2}} \frac{c_{\alpha+\beta}}{c_\beta s_\beta} + 4m_{A^0}^2 s_{\alpha-\beta} - 2m_{h^0}^2 \left( \frac{c_{\alpha+\beta}}{c_\beta s_\beta} + s_{\alpha-\beta} \right) \right\}, \\
g_{h^0 H^+ H^-} &= \sqrt{G_F} \left\{ \frac{M^2}{\sqrt{2}} \frac{c_{\alpha+\beta}}{c_\beta s_\beta} + 4m_{H^\pm}^2 s_{\alpha-\beta} - 2m_{h^0}^2 \left( \frac{c_{\alpha+\beta}}{c_\beta s_\beta} + s_{\alpha-\beta} \right) \right\}, \\
g_{H^0 h^0 h^0} &= \sqrt{G_F} \left\{ \frac{M^2}{\sqrt{2}} \left( -s_{\alpha+\beta} + 3 \frac{s_\alpha}{s_\beta} - 3 s_\alpha^2 \frac{s_{\alpha-\beta}}{s_\beta c_\beta} \right) - (4m_{h^0}^2 + 2m_{H^0}^2) \left( \frac{s_\alpha}{s_\beta} - s_\alpha^2 \frac{s_{\alpha-\beta}}{s_\beta c_\beta} \right) \right\}, \\
g_{H^0 A^0 A^0} &= \sqrt{G_F} \left\{ \frac{M^2}{\sqrt{2}} \frac{s_{\alpha+\beta}}{c_\beta s_\beta} - 4m_{A^0}^2 c_{\alpha-\beta} + 2m_{H^0}^2 \left( c_{\alpha-\beta} - \frac{s_{\alpha+\beta}}{c_\beta s_\beta} \right) \right\}, \\
g_{H^0 H^+ H^-} &= \sqrt{G_F} \left\{ \frac{M^2}{\sqrt{2}} \frac{s_{\alpha+\beta}}{c_\beta s_\beta} - 4m_{H^\pm}^2 c_{\alpha-\beta} + 2m_{H^0}^2 \left( c_{\alpha-\beta} - \frac{s_{\alpha+\beta}}{c_\beta s_\beta} \right) \right\}.
\end{aligned} \tag{11}$$

## B Higgs and gauge boson scattering amplitudes

The tree-level S-wave amplitudes for the scattering of Higgs and longitudinal gauge bosons in the high energy regime can be calculated elegantly using the equivalence theorem [20, 37]. We consider 14 distinct neutral channel scattering processes to be studied [21],

$$W_L^+ W_L^-, W_L^+ H^-, W_L^- H^+, H^+ H^-, Z_L Z_L, Z_L A, AA, Z_L h, Z_L H, Ah, AH, hh, hH, HH,$$

which lead to a 14-dimensional S-matrix, with the following eigenvalues, generically referred to as  $a_i (i = 1, \dots, 14)$ , expressed in terms of the parameters  $\lambda_i$  of the Higgs potential (1).

$$\begin{aligned}
a_{\pm} &= \frac{1}{16\pi} \left\{ 3(\lambda_1 + \lambda_2 + 2\lambda_3) \pm \sqrt{9(\lambda_1 - \lambda_2)^2 + (4\lambda_3 + \lambda_4 + \lambda_5/2 + \lambda_6/2)^2} \right\}, \\
b_{\pm} &= \frac{1}{16\pi} \left\{ \lambda_1 + \lambda_2 + 2\lambda_3 \pm \sqrt{(\lambda_1 - \lambda_2)^2 + (-2\lambda_4 + \lambda_5 + \lambda_6)^2/4} \right\}, \\
c_{\pm} &= d_{\pm} = \frac{1}{16\pi} \left\{ \lambda_1 + \lambda_2 + 2\lambda_3 \pm \sqrt{(\lambda_1 - \lambda_2)^2 + (\lambda_5 - \lambda_6)^2/4} \right\}, \\
e_1 &= \frac{1}{16\pi} \left\{ 2\lambda_3 - \lambda_4 - \lambda_5/2 + 5\lambda_6/2 \right\}, \\
e_2 &= \frac{1}{16\pi} \left\{ 2\lambda_3 + \lambda_4 - \lambda_5/2 + \lambda_6/2 \right\}, \\
f_+ &= \frac{1}{16\pi} \left\{ 2\lambda_3 - \lambda_4 + 5\lambda_5/2 - \lambda_6/2 \right\}, \\
f_- &= \frac{1}{16\pi} \left\{ 2\lambda_3 + \lambda_4 + \lambda_5/2 - \lambda_6/2 \right\}, \\
f_1 &= f_2 = \frac{1}{16\pi} \left\{ 2\lambda_3 + \lambda_5/2 + \lambda_6/2 \right\}.
\end{aligned} \tag{12}$$

In our study, we require the moduli of all these amplitudes to stay below 1/2 [8].

To obtain the S-wave amplitudes (12) in terms of masses and mixing angles in the Higgs sector, we eliminate  $\lambda_i (i = 1, 2, 3, 4, 6)$  according to the following relations.

$$\begin{aligned}
\lambda_1 &= \frac{\Sigma}{8v^2 c_{\beta}^2} + \frac{\Delta}{8v^2} \left( \frac{c_{2\alpha}}{c_{\beta}^2} - 2 \frac{s_{2\alpha}}{s_{2\beta}} \right) + \frac{\lambda_5}{4} \left( 1 - \tan^2 \beta \right), \\
\lambda_2 &= \frac{\Sigma}{8v^2 c_{\beta}^2} - \frac{\Delta}{8v^2} \left( \frac{c_{2\alpha}}{s_{\beta}^2} + 2 \frac{s_{2\alpha}}{s_{2\beta}} \right) + \frac{\lambda_5}{4} \left( 1 - \cot^2 \beta \right), \\
\lambda_3 &= \frac{\Delta}{4v^2} \frac{s_{2\alpha}}{s_{2\beta}} - \frac{\lambda_5}{4}, \quad \lambda_4 = \frac{m_{H^{\pm}}^2}{v^2}, \quad \lambda_6 = \frac{m_{A^0}^2}{v^2},
\end{aligned} \tag{13}$$

with  $\Sigma = m_{H^0}^2 + m_{h^0}^2$  and  $\Delta = m_{H^0}^2 - m_{h^0}^2$ .

## References

- [1] N. Arkani-Hamed, S. Dimopoulos and G. R. Dvali, Phys. Rev. D **59** (1999) 086004; Phys. Lett. B **429** (1998) 263.
- [2] N. Arkani-Hamed, A. G. Cohen and H. Georgi, Phys. Lett. B **513** (2001) 232; N. Arkani-Hamed, A.G. Cohen, E. Katz, and A.E. Nelson, JHEP **07** (2002) 034; M. Schmaltz, Nucl. Phys. Proc. Suppl. **117** (2003) 40; T. Han, H.E. Logan, B. McElrath, and L.-T. Wang, Phys. Rev. D **67** (2003) 095004.
- [3] H.-J. He, C.T. Hill, and T.M.P. Tait, Phys. Rev. D **65** (2002) 055006.
- [4] S. Weinberg, Phys. Rev. Lett. **37** (1976) 657.
- [5] A. Zee, Phys. Lett. B **93** (1980) 389 [Erratum-ibid. **95** (1980) 461]; S. Kanemura, T. Kasai, G.-L. Lin, Y. Okada, J.-J. Tseng, and C.-P. Yuan, Phys. Rev. D **64** (2001) 053007; K. Cheung and O. Seto, Phys. Rev. D **69** (2004) 113009.
- [6] A.G. Cohen, D.B. Kaplan, A.E. Nelson, Ann. Rev. Nucl. Part. Sci. **43** (1993) 27 A.T. Davies, C.D. Froggatt, G. Jenkins, R.G. Moorhouse, Phys. Lett. B **336** (1994) 464; K. Funakubo, A. Kakuto, K. Takenaga, Prog. Theor. Phys. **91** (1994) 341; J.M. Cline, K. Kainulainen, A.P. Vischer, Phys. Rev. D **54** (1996) 2451; S. Kanemura, Y. Okada and E. Senaha, Phys. Lett. B **606** (2005) 361.
- [7] S. Glashow and S. Weinberg, Phys. Rev. D **15** (1977) 1958.
- [8] J.F. Gunion, H.E. Haber, G. L. Kane, S. Dawson, *The Higgs Hunter's Guide*, Addison-Wesley Publishing Company, 1990 [Erratum hep-ph/9302272].
- [9] A. C. Bawa, C. S. Kim and A. D. Martin, Z. Phys. C **47** (1990) 75;
- [10] J. F. Gunion, H. E. Haber, F. E. Paige, W. K. Tung and S. S. D. Willenbrock, Nucl. Phys. B **294** (1987) 621.
- [11] D. A. Dicus, J. L. Hewett, C. Kao and T. G. Rizzo, Phys. Rev. D **40** (1989) 787.
- [12] A. A. Barrientos Bendezú and B. A. Kniehl, Phys. Rev. D **59** (1999) 015009; ibid. D **61** (2000) 097701; ibid. D **63** (2001) 015009.
- [13] O. Brein, W. Hollik and S. Kanemura, Phys. Rev. D **63** (2001) 095001.
- [14] F. Zhou, W. G. Ma, Y. Jiang, L. Han and L. H. Wan, Phys. Rev. D **63** (2001) 015002.
- [15] Y. S. Yang, C. S. Li, L. G. Jin and S. H. Zhu, Phys. Rev. D **62** (2000) 095012.

- [16] W. Hollik and S. H. Zhu, Phys. Rev. D **65** (2002) 075015.
- [17] S. Moretti and K. Odagiri, Phys. Rev. D **59** (1999) 055008.
- [18] N.G. Deshpande and E. Ma, Phys. Rev. D **18** (1978) 2574.
- [19] S. Nie and M. Sher, Phys. Lett. B **449** (1999) 89; S. Kanemura, T. Kasai, and Y. Okada, Phys. Lett. B **471** (1999) 182.
- [20] B.W. Lee, C. Quigg, and H.B. Thacker, Phys. Rev. Lett. **38** (1977) 883; Phys. Rev. D **16** (1977) 1519.
- [21] S. Kanemura, T. Kubota, and E. Takasugi, Phys. Lett. B **313** (1993) 155.
- [22] H. Hüffel and G. Pocsik, Z. Phys. C **8** (1981) 13; J. Maalampi, J. Sirkka, and I. Vilja, Phys. Lett. B **265** (1991) 371; A. Akeroyd, A. Arhrib, and E.-M. Naimi, Phys. Lett. B **490** (2000) 119; I.F. Ginzburg and I.P. Ivanov, arXiv:hep-ph/0312374.
- [23] S. Kanemura, Eur. Phys. J. C **17** (2000) 473; S. Kanemura, S. Kiyoura, Y. Okada, E. Senaha and C. P. Yuan, Phys. Lett. B **558** (2003) 157; S. Kanemura, Y. Okada, E. Senaha and C. P. Yuan, Phys. Rev. D **70** (2004) 115002.
- [24] P. Koppenburg *et al.*, the Belle Collaboration, Phys. Rev. Lett. **93** (2004) 061803.
- [25] M. Ciuchini, G. Degrassi, P. Gambini, and G.F. Giudice, Nucl. Phys. B **527** (1998) 21; P. Ciafaloni, A. Romanino, and A. Strumia, Nucl. Phys. B **524** (1998) 361; F. Borzumati and G. Greub, Phys. Rev. D **58** (1998) 074004; T.M. Aliev and E.O. Iltan, Phys. Rev. D **58** (1998) 095014.
- [26] O. Brein, Ph.D. Thesis, University of Karlsruhe (2002), Rhombos-Verlag, Berlin 2002; O. Brein in: *SUSY 02, the 10th Int. Conf. on Supersymmetry and Unification of Fundamental Interactions*, Vol. 2, DESY Hamburg, 2002, eds. P. Nath and P. Zerwas [hep-ph/0209124].
- [27] S. Eidelman *et al.* [Particle Data Group Collaboration], Phys. Lett. B **592** (2004) 1.
- [28] J. Abdallah *et al.* [DELPHI Collaboration], Eur. Phys. J. C **32** (2004) 145.
- [29] G. W. Bennett *et al.* [Muon g-2 Collaboration], Phys. Rev. Lett. **89** (2002) 101804 [Erratum-ibid. **89** (2002) 129903]; *ibid.* **92** (2004) 161802.
- [30] D. Toussaint, Phys. Rev. D **18** (1978) 1626; S. Bertolini, Nucl. Phys. B **272** (1986) 77; W. Hollik, Z. Phys. C **32** (1986) 291; *ibid.* C **37** (1988) 569; A. Denner, R. J. Guth and J. H. Kühn, Phys. Lett. B **240** (1990) 438.

- [31] J. Küblbeck, M. Böhm and A. Denner, *Comput. Phys. Commun.* **60** (1990) 165; H. Eck, Ph.D. thesis, University of Würzburg (1995); T. Hahn and M. Perez-Victoria, *Comput. Phys. Commun.* **118** (1999) 153; T. Hahn, *Comput. Phys. Commun.* **140** (2001) 418.
- [32] R. Brock *et al.* [CTEQ Collaboration], *Handbook of perturbative QCD: Version 1.0*, *Rev. Mod. Phys.* **67** (1995) 157.
- [33] A. D. Martin, R. G. Roberts, W. J. Stirling and R. S. Thorne, *Eur. Phys. J. C* **4** (1998) 463.
- [34] J. P. Leveille, *Nucl. Phys. B* **137** (1978) 63; H. E. Haber, G. L. Kane and T. Sterling, *Nucl. Phys. B* **161** (1979) 493; A. Dedes and H. E. Haber, *JHEP* **0105** (2001) 006, hep-ph/0102297.
- [35] J. D. Bjorken and S. Weinberg, *Phys. Rev. Lett.* **38** (1977) 622; S. M. Barr and A. Zee, *Phys. Rev. Lett.* **65** (1990) 21 [Erratum-*ibid.* **65** (1990) 2920].
- [36] D. Chang, W. F. Chang, C. H. Chou and W. Y. Keung, *Phys. Rev. D* **63** (2001) 091301; K. m. Cheung, C. H. Chou and O. C. W. Kong, *Phys. Rev. D* **64** (2001) 111301; A. Arhrib and S. Baek, *Phys. Rev. D* **65** (2002) 075002; M. Krawczyk, hep-ph/0103223.
- [37] J. M. Cornwall, D. N. Levin and G. Tiktopoulos, *Phys. Rev. Lett.* **30** (1973) 1268 [Erratum-*ibid.* **31** (1973) 572]; *Phys. Rev. D* **10** (1974) 1145 [Erratum-*ibid.* **11** (1975) 972]; M. S. Chanowitz and M. K. Gaillard, *Nucl. Phys. B* **261** (1985) 379; Y. P. Yao and C. P. Yuan, *Phys. Rev. D* **38** (1988) 2237; H. G. J. Veltman, *Phys. Rev. D* **41** (1990) 2294; J. Bagger and C. Schmidt, *Phys. Rev. D* **41** (1990) 264; H. J. He, Y. P. Kuang and X. y. Li, *Phys. Rev. Lett.* **69** (1992) 2619,

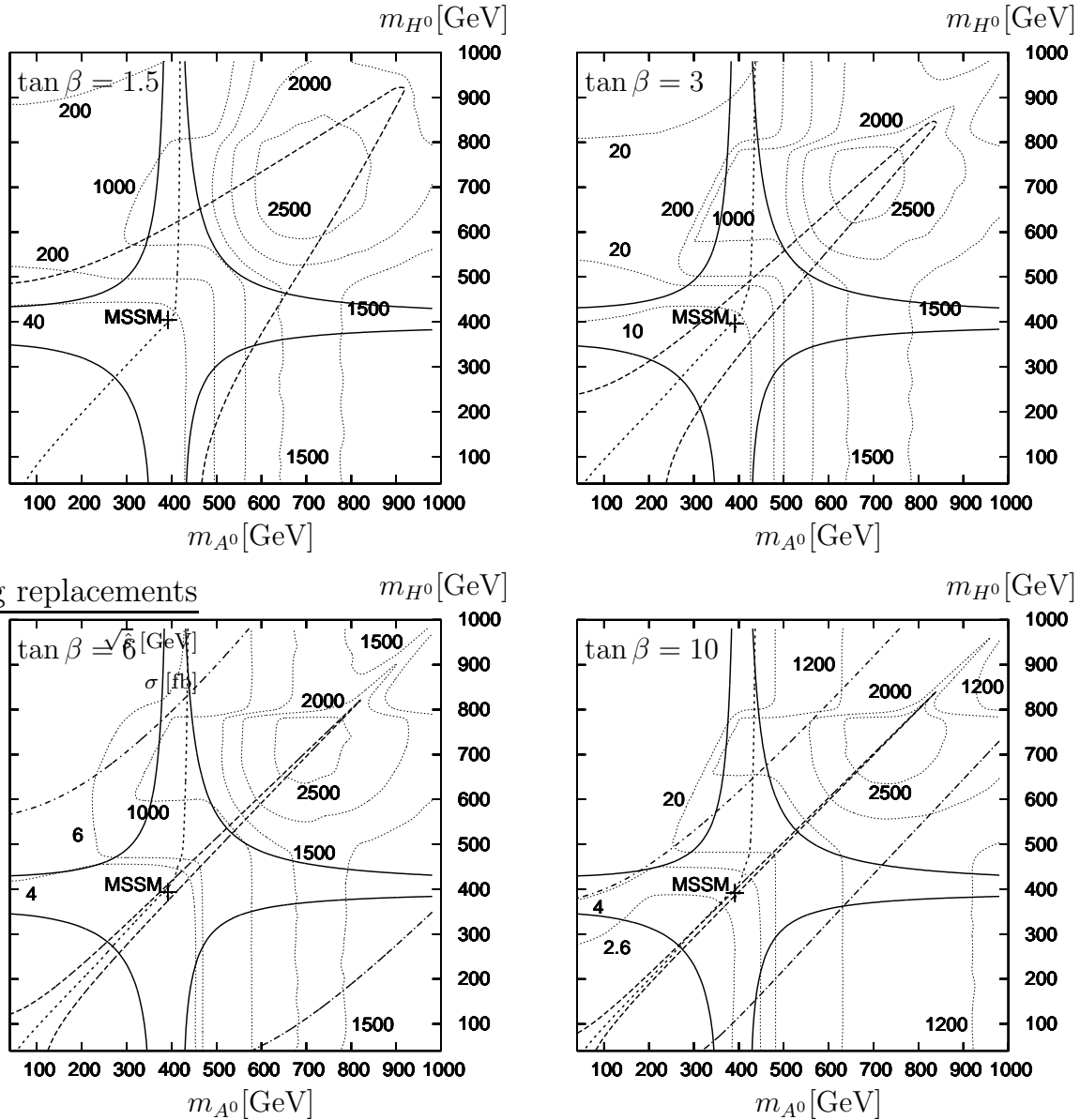


Figure 3: Contour of the Hadronic cross section  $\sigma_{pp \rightarrow W^\pm H^\mp}$  in fb for the case  $M^2 = m_{A^0}^2$  (thin dotted lines). The limiting contours for  $\delta\rho_0$  (thick solid lines) allow the cross-shaped area, and for  $\delta a_\mu$  (thick dot-dashed lines) the whole displayed area for  $\tan\beta = 1.5, 3$  and the band-shaped area for  $\tan\beta = 6, 10$ . The perturbative unitarity constraint,  $\max|a_i| < 1/2$ , (thick dashed lines) allows the pointed area which includes the lower left corner. The area allowed by the vacuum stability condition (2) is left of the thick short-dashed contour. The cross, labeled “MSSM”, shows the point where all Higgs sector parameters coincide with the ones of our reference MSSM scenario.

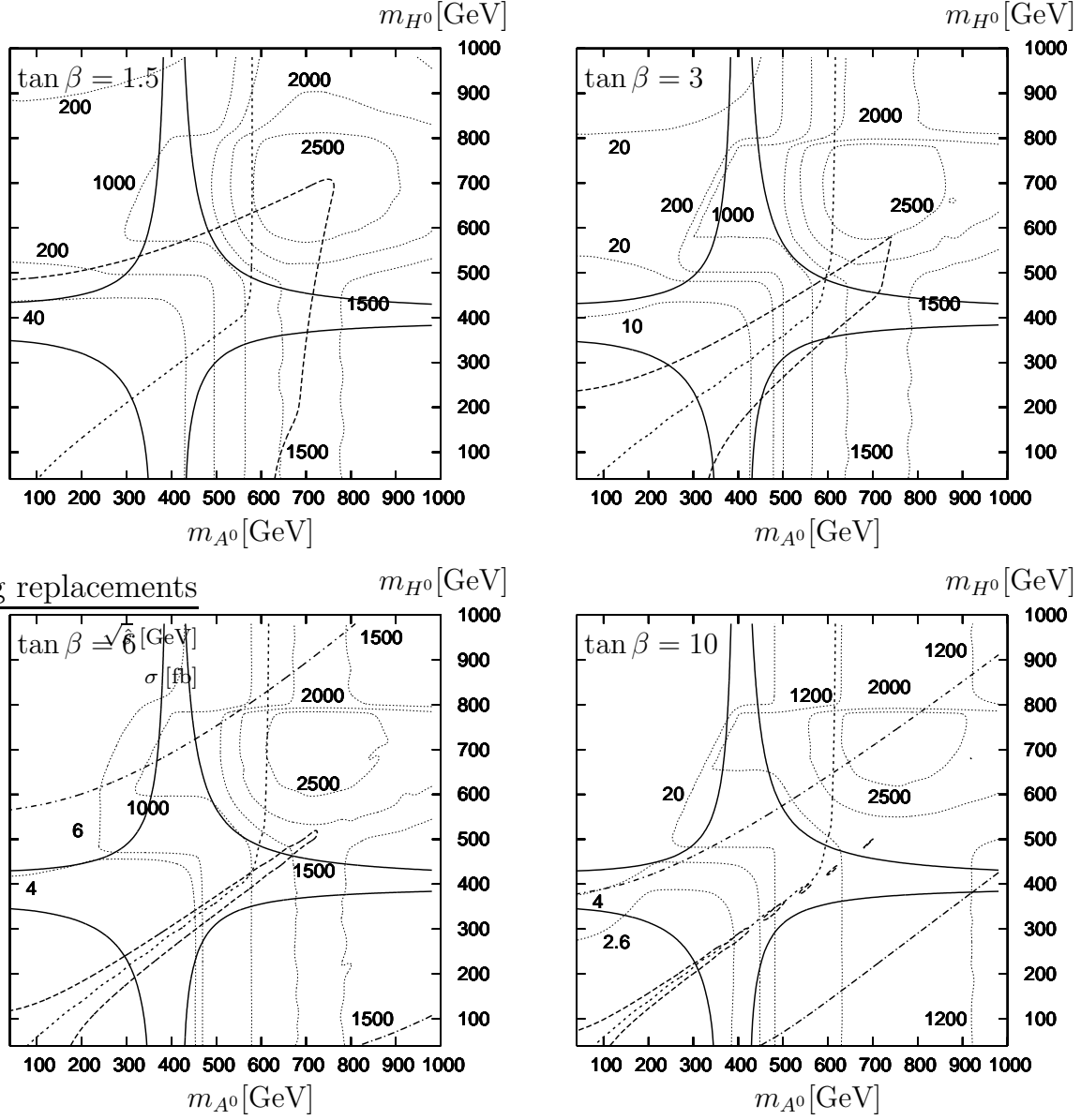


Figure 4: Contour of the Hadronic cross section  $\sigma_{pp \rightarrow W^\pm H^\mp}$  in fb for the case  $M^2 = m_{A^0}^2/2$  (thin dotted lines). The area of allowed parameter space, defined by the superposition of limiting contours for  $\delta\rho_0$  (thick solid lines),  $\delta a_\mu$  (thick dot-dashed lines), perturbative unitarity (thick dashed lines), and vacuum stability (thick short-dashed lines), is described in Fig. 3.

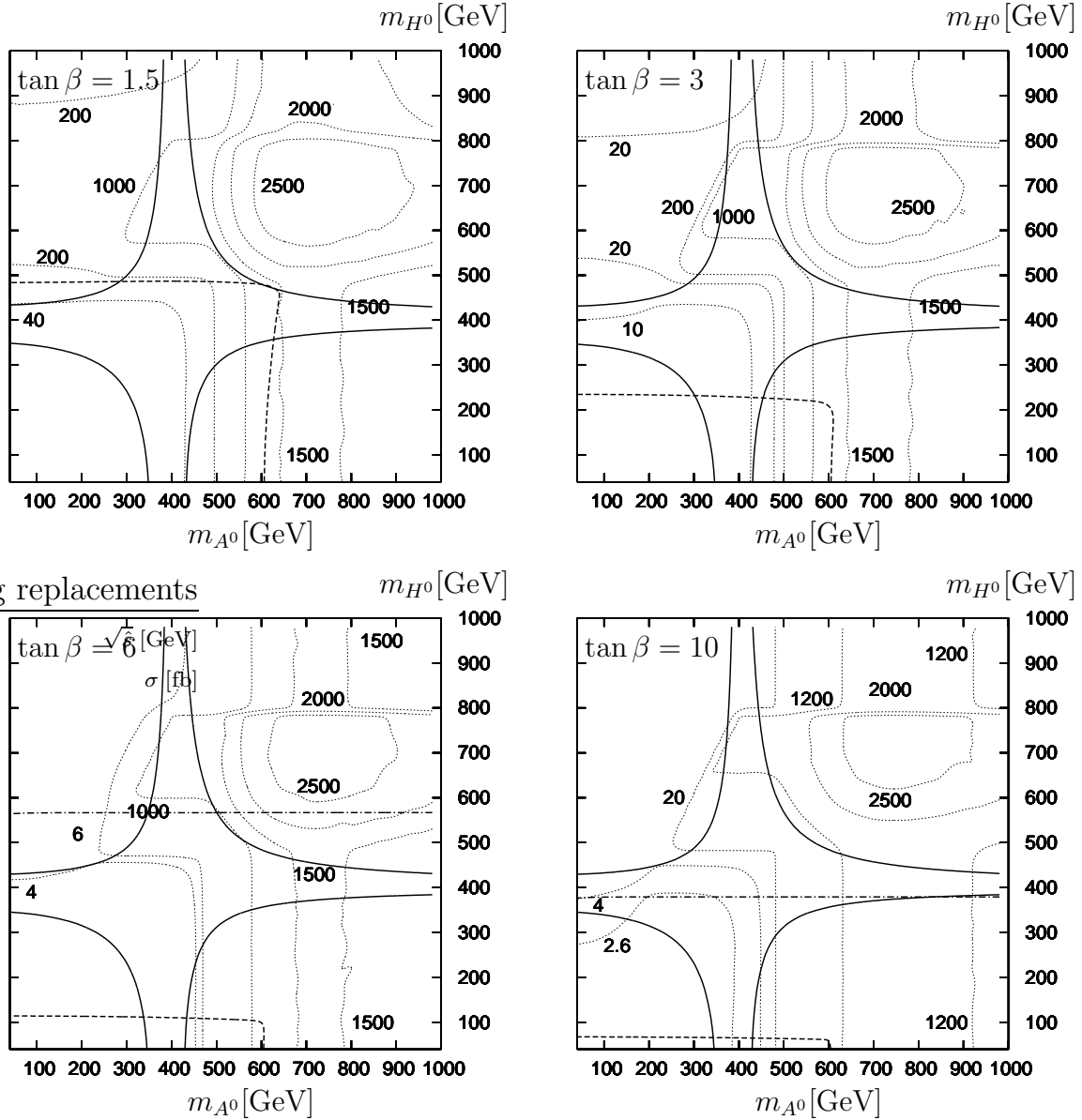


Figure 5: Contour of the Hadronic cross section  $\sigma_{pp \rightarrow W^\pm H^\mp}$  in fb for the case  $M^2 = 0$  (thin dotted lines). The limiting contours for the allowed values of  $\delta\rho_0$  (thick solid lines) allows the cross-shaped area, for  $\delta a_\mu$  the whole displayed area for  $\tan\beta = 1.5, 3$  and the area below the thick dot-dashed line for  $\tan\beta = 6, 10$ . The perturbative unitarity constraint,  $\max|a_i| < 1/2$ , (thick dashed lines) allows the almost rectangular area which includes the lower left corner. The vacuum stability condition (2) gives no constraint on the displayed area.